Haverford College

Haverford Scholarship

Faculty Publications

Astronomy

2013

Dense Molecular Gas: A Sensitive Probe of Stellar Feedback Models

P. F. Hopkins

Desika Narayanan
Haverford College, dnarayan@haverford.edu

Follow this and additional works at: https://scholarship.haverford.edu/astronomy_facpubs

Repository Citation

Dense molecular gas: a sensitive probe of stellar feedback models

Philip F. Hopkins,[1]* Desika Narayanan,[2] Norman Murray[3]† and Eliot Quataert[1]

[1]*Department of Astronomy and Theoretical Astrophysics Center, University of California Berkeley, Berkeley, CA 94720, USA*
[2]*Steward Observatory, University of Arizona, 933 North Cherry Avenue, Tucson, AZ 85721, USA*
[3]*Canadian Institute for Theoretical Astrophysics, 60 St. George Street, University of Toronto, ON M5S 3H8, Canada*

ABSTRACT

We show that the mass fraction of giant molecular cloud (GMC) gas ($n \gtrsim 100\,\mathrm{cm}^{-3}$) in dense ($n \gg 10^4\,\mathrm{cm}^{-3}$) star-forming clumps, observable in dense molecular tracers ($L_{\mathrm{HCN}}/L_{\mathrm{CO(1-0)}}$), is a sensitive probe of the strength and mechanism(s) of stellar feedback, as well as the star formation efficiencies in the most dense gas. Using high-resolution galaxy-scale simulations with pc-scale resolution and explicit models for feedback from radiation pressure, photoionization heating, stellar winds and supernovae (SNe), we make predictions for the dense molecular gas tracers as a function of GMC and galaxy properties and the efficiency of stellar feedback/star formation. In models with weak/no feedback, much of the mass in GMCs collapses into dense subunits, predicting $L_{\mathrm{HCN}}/L_{\mathrm{CO(1-0)}}$ ratios order-of-magnitude larger than observed. By contrast, models with feedback properties taken directly from stellar evolution calculations predict dense gas tracers in good agreement with observations. Changing the strength or timing of SNe tends to move systems along, rather than off, the L_{HCN}–L_{CO} relation (because SNe heat lower density material, not the high-density gas). Changing the strength of radiation pressure (which acts efficiently in the highest density gas), however, has a much stronger effect on L_{HCN} than on L_{CO}. We show that degeneracies between the strength of feedback, and efficiency of star formation on small scales, can be broken by the combination of dense gas, intermediate-density gas and total star formation rate (SFR) tracers, and favour models where the galaxy-integrated star formation efficiency in dense gas is low. We also predict that the fraction of dense gas ($L_{\mathrm{HCN}}/L_{\mathrm{CO(1-0)}}$) increases with increasing GMC surface density; this drives a trend in $L_{\mathrm{HCN}}/L_{\mathrm{CO(1-0)}}$ with SFR and luminosity which has tentatively been observed. Our results make specific predictions for enhancements in the dense gas tracers in unusually dense environments such as ultraluminous infrared galaxies and galactic nuclei (including the galactic centre).

Key words: galaxies: active – galaxies: evolution – galaxies: formation – galaxies: star formation – cosmology: theory.

1 INTRODUCTION

Feedback from massive stars is critical to the evolution of galaxies, the properties and structure of the interstellar medium (ISM) and the formation of stars and star clusters in giant molecular clouds (GMCs). The Kennicutt–Schmidt law for star formation (SF) in galaxies implies a gas consumption time of ∼50 dynamical times (Kennicutt 1998). Moreover, the total fraction of the gas turned into stars in GMCs over their lifetime is only a few per cent (Zuckerman & Evans 1974; Williams & McKee 1997; Evans 1999; Evans et al. 2009).

In an instantaneous sense, the low star formation rate (SFR) in GMCs is closely related to the fact that most of the gas within GMCs is at relatively low densities $n \sim 10$–$100\,\mathrm{cm}^{-3}$, i.e. *not* in star-forming cores that have densities $\gtrsim 10^4\,\mathrm{cm}^{-3}$ (e.g. Williams & McKee 1997; Evans 1999, and references therein). Tracers of high-density gas such as the HCN transition (critical density $n \gtrsim 10^4\,\mathrm{cm}^{-3}$) have shown that it is the gas at these high densities that is actually forming stars – what determines the SFR in GMCs is the amount of mass at these densities (e.g. Shirley et al. 2003; Wu et al. 2005; Lada, Lombardi & Alves 2010). In typical GMCs, this is ∼10 per cent of the mass, but SF is relatively rapid in the clumps, giving the canonical SFR of a few per cent of the GMC mass per dynamical time.

Furthermore, observations have suggested that in high-density systems such as local merger-induced starbursts – which are known

* E-mail: phopkins@astro.berkeley.edu
† Canada Research Chair in Astrophysics.

to have a higher ratio of SFR to gas surface densities $\Sigma_{\rm sfr}/\Sigma_{\rm gas}$ (Kennicutt 1998) – have systematically higher ratios of high density to total gas mass (Gao & Solomon 2004b; Narayanan et al. 2005; Evans et al. 2006; Bussmann et al. 2008; Wu et al. 2010). The systematic increase of this ratio with surface density $\Sigma_{\rm gas}$ has been proposed as the origin of the difference between the apparently linear SFR–dense gas mass relation (which follows if the mass at a specific high density has a high, constant SF efficiency) and the superlinear Kennicutt–Schmidt relation (Gao & Solomon 2004b; Wu et al. 2005; Krumholz & Thompson 2007, but see also Yao et al. 2003; Narayanan, Cox & Hernquist 2008a; Narayanan et al. 2008b).

Exactly what determines the amount of dense gas, and hence the SFR, remains unknown. In simulations without stellar feedback, GMCs experience runaway collapse to densities much higher than observed, and rapidly turn a near-unity fraction of their gas into stars (Bournaud et al. 2010; Dobbs, Burkert & Pringle 2011; Harper-Clark & Murray 2011; Hopkins, Quataert & Murray 2011; Krumholz, Klein & McKee 2011; Tasker 2011). Neither thermal pressure nor turbulence in and of itself can stave off collapse in the ISM: cooling is rapid, so that thermal support is quickly lost, and turbulent support dissipates on a single crossing time (e.g. Ostriker, Stone & Gammie 2001). Some mechanism must therefore continuously inject energy and momentum into the gas on both GMC and galactic scales, in order to prevent runaway collapse to arbitrarily high densities.

Various physical mechanisms have been proposed as a source of random motions in GMCs: photoionization, stellar winds, radiation pressure from ultraviolet (UV) and infrared (IR) photons, protostellar jets, cosmic rays, supernovae and gravitational cascades from large scales (e.g. Mac Low & Klessen 2004, and references therein). In Hopkins et al. (2011, hereafter Paper I) and Hopkins, Quataert & Murray (2012a, hereafter Paper II), we therefore developed a library of numerical hydrodynamic simulations of galaxies, with pc-scale resolution, molecular cooling and explicit spatial/time resolution of feedback mechanisms including radiation pressure in the UV and IR, supernovae, massive and asymptotic giant branch (AGB) stellar winds and H II photoionization heating. In Papers I and II, we show that these feedback mechanisms generically lead to the formation of a self-regulating, quasi-steady-state multiphase ISM, in which dense GMCs form via gravitational collapse. Gas inside these GMCs then forms parsec scale clumps at densities $n > 10^4\,{\rm cm}^{-3}$ in which most stars form; the GMCs hosting these clumps are then quickly broken up by feedback after they turn a few per cent of their mass into stars.

We showed in Paper II that most properties of the ISM and GMCs are insensitive to the strength and precise mechanisms of feedback, so long as *sufficient* feedback is present to resist runaway dissipation and collapse. But this is largely a property of the low-density (non-star-forming) gas in GMCs – their properties are set to be those of any marginally self-gravitating object, i.e. they trace the Jeans mass and collapse conditions (Hopkins 2012). The gas at high densities can, in principle, evolve very far away from its 'initial' conditions even in just a couple GMC dynamical times. In this paper, we investigate the consequences of different feedback mechanisms for the dense gas in galaxies and GMCs.

2 THE SIMULATIONS

The simulations used here are described in detail in Paper I (section 2 and tables 1–3) and Paper II (section 2). We briefly summarize the most important properties here. The simulations were performed with the parallel TreeSPH code GADGET-3 (Springel 2005). They include stars, dark matter and gas, with cooling, SF and stellar feedback.

Gas follows an atomic cooling curve with additional fine-structure cooling to <100 K, with no 'cooling floor' imposed. SF is allowed only in dense regions above $n > 1000\,{\rm cm}^{-3}$, at a rate $\dot{\rho}_* = \epsilon_* \, \rho_{\rm mol}/t_{\rm ff}$, where $t_{\rm ff}$ is the free-fall time, $\rho_{\rm mol} = f_{\rm H_2}\,\rho$ is the molecular gas density and $\epsilon_* = 1.5$ per cent is a nominal efficiency at these densities (Krumholz & Tan 2007). We follow Krumholz & Gnedin (2011) to calculate the molecular fraction $f_{\rm H_2}$ in dense gas as a function of local column density and metallicity. In Papers I and II we show that the galaxy structure and SFR are basically independent of the small-scale SF law (independent of ϵ_* in particular), density threshold (provided it is high) and treatment of molecular chemistry. However, we discuss below how the properties of the most dense gas depend on these prescriptions.

Stellar feedback is included, via a variety of mechanisms.

(1) *Local momentum flux from radiation pressure, supernovae and stellar winds.* Gas within a GMC (identified with an on-the-fly friends-of-friends algorithm) receives a direct momentum flux from the stars in that cluster/clump. The momentum flux is $\dot{P} = \dot{P}_{\rm SNe} + \dot{P}_{\rm w} + \dot{P}_{\rm rad}$, where the separate terms represent the direct momentum flux of SNe ejecta, stellar winds and radiation pressure. The first two are directly tabulated for a single stellar population as a function of age and metallicity Z and the flux is directed away from the stellar centre. Because the local momentum flux is, by definition in our simulations, interior to clouds, the systems are always optically thick to UV radiation, so the radiation force is approximately $\dot{P}_{\rm rad} \approx (1 + \tau_{\rm IR})\,L_{\rm incident}/c$, where $1 + \tau_{\rm IR} = 1 + \Sigma_{\rm gas}\,\kappa_{\rm IR}$ accounts for the absorption of the initial UV/optical flux and multiple scatterings of the IR flux if the region is optically thick in the IR (with $\Sigma_{\rm gas}$ calculated for each particle given its location in the GMC).

(2) *Supernova shock-heating.* Gas shocked by supernovae can be heated to high temperatures. We tabulate the SNe Type I and Type II rates from Mannucci, Della Valle & Panagia (2006) and STARBURST99, respectively, as a function of age and metallicity for all star particles and stochastically determine at each time-step if a SN occurs. If so, the appropriate mechanical luminosity is injected as thermal energy in the gas within a smoothing length (nearest 32 gas neighbours) of the star particle.

(3) *Gas recycling and shock-heating in stellar winds.* Gas mass is returned to the ISM from stellar evolution, at a rate tabulated from SNe and stellar mass loss (integrated fraction ≈0.3). The SNe heating is described above. Similarly, stellar winds are assumed to shock locally and inject the appropriate tabulated mechanical luminosity $L(t, Z)$ as a function of age and metallicity into the gas within a smoothing length.

(4) *Photoheating of H II regions.* We also tabulate the rate of production of ionizing photons for each star particle; moving radially outwards from the star, we then ionize each neutral gas particle (using its density and state to determine the necessary photon number) until the photon budget is exhausted. Ionized gas is maintained at a minimum $\sim 10^4$ K until it falls outside an H II region.

(5) *Long-range radiation pressure.* Photons which escape the local GMC [not accounted for in mechanism (1) above] can be absorbed at larger radii. Knowing the intrinsic spectral energy distribution (SED) of each star particle, we attenuate integrating the local gas density and gradients to convergence. The resulting 'escaped' SED gives a flux that propagates to large distances, and can be treated in the same manner as the gravity tree to give the local

net incident flux on a gas particle. The local absorption is then calculated integrating over a frequency-dependent opacity that scales with metallicity, and the radiation pressure force is imparted.

In implementing (1)–(5), all energy, mass and momentum-injection rates are taken from stellar population models (Leitherer et al. 1999), assuming a Kroupa (2002) initial mass function (IMF), without any free parameters. More details, numerical tests and resolution studies for these models are discussed in Paper II; some additional numerical tests are discussed in Appendix A.

We implement the model in four distinct initial disc models spanning a range of galaxy types. Each has a bulge, stellar and gaseous disc, halo and central black hole (BH; although to isolate the role of stellar feedback, models for BH growth and feedback are disabled). At our standard resolution, each model has ~ 0.3–1×10^8 total particles, giving particle masses of 500–1000 $M_\odot$ and 1–5 pc smoothing lengths, and are run for a few orbital times each. A couple ultrahigh resolution runs for convergence tests employ $\sim 10^9$ particles with sub-pc resolution. The disc models include the following.

(1) Small Magellanic Cloud (SMC): an SMC-like dwarf, with baryonic mass $M_{\rm bar} = 8.9 \times 10^8 \, M_\odot$ (gas $m_{\rm g} = 7.5 \times 10^8 \, M_\odot$, bulge $M_{\rm b} = 1.3 \times 10^8 \, M_\odot$, the remainder in a stellar disc $m_{\rm d}$) and halo mass $M_{\rm halo} = 2 \times 10^{10} \, M_\odot$. The gas (stellar) scale length is $h_{\rm g} = 2.1$ kpc ($h_{\rm d} = 0.7$).

(2) Milky Way (MW): a MW-like galaxy, with halo $M_{\rm halo} = 1.6 \times 10^{12}$, and baryonic ($M_{\rm bar}, m_{\rm b}, m_{\rm d}, m_{\rm g}) = (7.1, 1.5, 4.7, 0.9) \times 10^{10} \, M_\odot$ with scale-lengths ($h_{\rm d}, h_{\rm g}) = (3.0, 6.0)$ kpc.

(3) Sbc: a gas-rich dwarf starburst disc with halo $M_{\rm halo} = 1.5 \times 10^{11}$, and baryonic ($M_{\rm bar}, m_{\rm b}, m_{\rm d}, m_{\rm g}) = (10.5, 1.0, 4.0, 5.5) \times 10^9 \, M_\odot$ with scale-lengths ($h_{\rm d}, h_{\rm g}) = (1.3, 2.6)$ kpc.

(4) HiZ: a high-redshift massive starburst disc (typical of intermediate SMGs at $z \sim 2$–4); $M_{\rm halo} = 1.4 \times 10^{12} \, M_\odot$ (scaled for $z = 2$ haloes), and baryonic ($M_{\rm bar}, m_{\rm b}, m_{\rm d}, m_{\rm g}) = (10.7, 0.7, 3, 7) \times 10^{10} \, M_\odot$ with scale-lengths ($h_{\rm d}, h_{\rm g}) = (1.6, 3.2)$ kpc.

3 HIGH-DENSITY GAS AND FEEDBACK

In Fig. 1, we plot the distribution of cold gas ($T < 1000$ K, mostly in GMCs) densities in each simulation. We show this for models with various feedback mechanisms enabled or disabled in turn. The basic properties of the 'standard' model (all feedback enabled) are discussed in Paper II: the distribution has a lognormal core (dispersion ~ 1–1.5 dex) with median $\langle n \rangle \sim 100 \, {\rm cm}^{-3}$, in good agreement with observations. As discussed in Section 1, the behaviour of this 'core' is not very sensitive to the model – they are just set by the conditions for gravitational collapse in a turbulent ($Q \sim 1$) disc (see Hopkins 2012). The *average* GMC properties (sizes, linewidths, densities, etc.) are not sensitive tracers of feedback.

But the high-n tail shows significant differences between models. Turning off feedback entirely leads to runaway collapse with a large secondary peak at $n \to 10^6 \, {\rm cm}^{-3}$ (the maximum resolved density). Turning off 'heating' mechanisms (shock-heating by SNe and stellar winds and photoionization heating) leads to a small increase in the amount of high-density $n \gtrsim 10^4 \, {\rm cm}^{-3}$ material in the MW and SMC models. But in all models, even the MW and SMC cases – where we show in Paper II that SNe heating may dominate the *global* self-regulation of the disc and generation of galactic winds (Hopkins, Quataert & Murray 2012b) – turning off radiation pressure (while still keeping SNe, stellar wind and photoheating) yields a much more dramatic increase in the amount of very dense material. In the HiZ and Sbc models, this is nearly as significant as turning off all feedback. In other words, even where global self-regulation can be
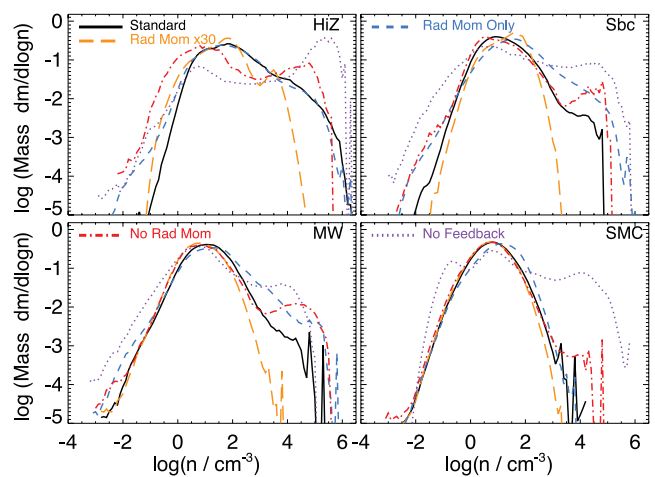

Figure 1. Distribution of 'cold' ($T < 1000$ K) gas densities n in each of the different disc galaxy models, with different feedback mechanisms (Section 2) enabled. 'Standard' means all mechanisms are included. In the 'no feedback' case, gas piles up at $n \gg 10^4 \, {\rm cm}^{-3}$. Even though SNe can regulate the *global* galaxy properties, including just thermal feedback mechanisms (SNe and stellar wind shock-heating and H II photoionization) without radiation pressure or momentum flux ('no momentum flux') leads to a similar excess at high n. Removing the heating mechanisms while keeping the radiation pressure ('rad mom only') has a modest effect on the high-n gas, even though it can dramatically change the galaxy wind and thermal state. If we make feedback stronger by simply increasing the strength of the radiation pressure momentum flux by a factor of 30, the amount of high-n material is strongly suppressed. Remarkably, these changes have almost no effect on the median densities of cold gas ($n \sim 10$–100 cm^{-3}) – i.e. typical densities of gas in GMCs – or the corresponding GMC mass function and linewidths (nor do they much alter the galaxy gas velocity dispersion or disc scale height; see Paper II). It is the dense gas that traces the effects of feedback.

set by SNe heating, the dense material at $n \gtrsim 10^4 \, {\rm cm}^{-3}$ is regulated by radiation pressure. This should be expected: at these densities optical depths are large in the infrared, and cooling times for SNe remnants are $\sim 10^4$ times shorter than the dynamical time.

We illustrate how this very dense gas can function as a tracer of the strength of radiation pressure by also comparing a series of otherwise identical models where we simply multiply the local radiation pressure force applied by a large, constant factor $\eta_p = 30$ everywhere in the simulation. Again, the median $\langle n \rangle$ is similar in both cases. However, to maintain global equilibrium, the boosted-feedback model requires much lower SFRs (and mass in young stars). In turn, the high-n tail (where stars actually form) is much smaller.

4 COMPARISON WITH OBSERVATIONS

In Fig. 2, we consider what these differences mean in terms of observational tracers. The total mass budget in intermediate-density molecular gas, roughly gas with $n \gtrsim 100 \, {\rm cm}^{-3}$, is commonly traced by the CO(1–0) transition. Since we know the mass in gas above this density, we can use the observed relation $M_{\rm mol} \approx 4.8 \, L_{\rm CO(1-0)}/({\rm K \, km \, s}^{-1} \, {\rm pc}^2)$ (Young & Scoville 1991) to estimate $L_{\rm CO}$. Similarly, the HCN luminosity $L_{\rm HCN}$ is related to the mass above its critical density, $n_{\rm crit} \approx 6 \times 10^4 \, {\rm cm}^{-3}$, as $M(n > n_{\rm crit}) \approx 5.5 \, L_{\rm HCN}/({\rm K \, km \, s}^{-1} \, {\rm pc}^2)$ (Gao & Solomon 2004a). Another high-density tracer is CO(3–2), with $n_{\rm crit} \approx 1.5 \times 10^4 \, {\rm cm}^{-3}$ and $M(n > n_{\rm crit}) \approx 1.33 \, L_{\rm CO(3-2)}/({\rm K \, km \, s}^{-1} \, {\rm pc}^2)$ (Narayanan et al. 2005). All of these conversions are uncertain at the factor of ~ 2 level, but
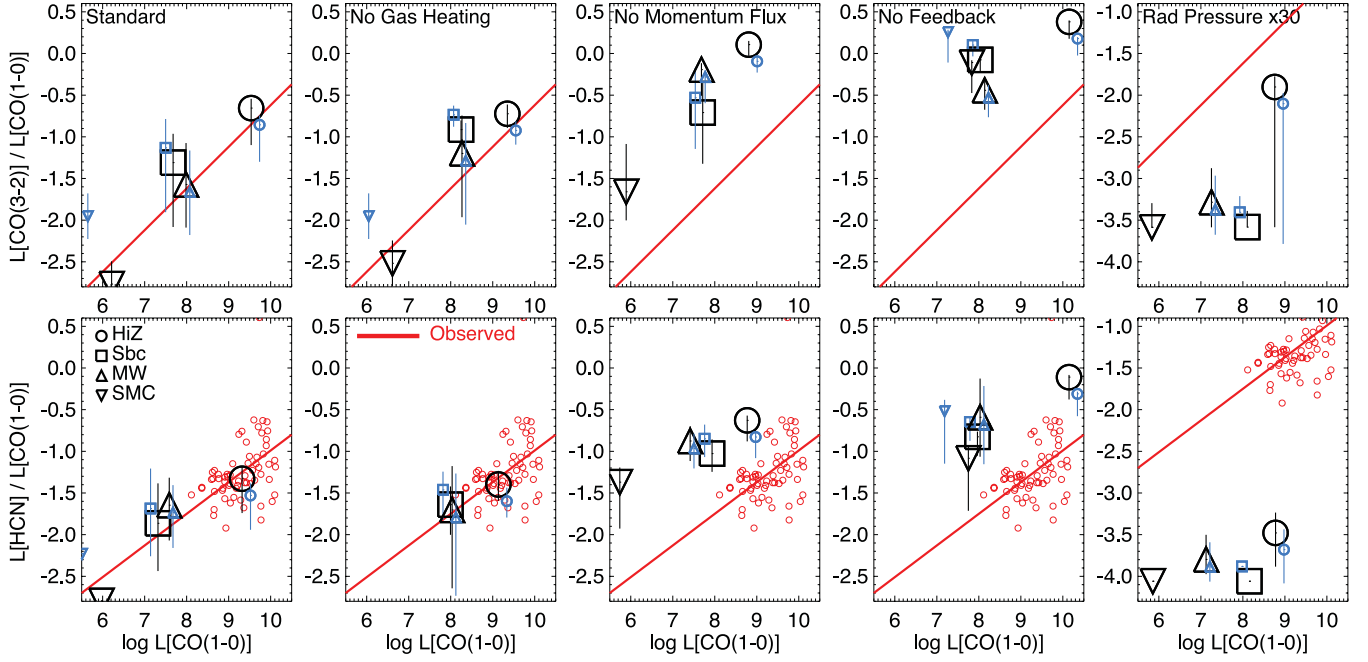
Figure 2. Dependence of observational dense-gas tracers on feedback and galaxy properties. We show the predicted ratio of the luminosity in HCN(1–0) (bottom) and CO(3–2) (top), with critical densities $n_{crit} \sim 6 \times 10^4, 1.5 \times 10^4\,cm^{-3}$, to the luminosity in CO(1–0), which traces the total molecular/GMC mass ($n \gtrsim 100\,cm^{-3}$). This is a proxy for the ratio of very dense star-forming gas, to total GMC mass, as a function of gas mass/SFR. The median and scatter in time for each galaxy model is plotted (points with error bars). Large black points adopt a constant α_{CO}, small blue points adopt $\alpha_{CO}(\Sigma_{H_2}, Z)$ from Narayanan et al. (2012). The observed best-fitting trend (line) and data points (small circles) are taken from Gao & Solomon (2004a). We compare models with different feedback mechanisms, as Fig. 1: our standard model; no gas heating from SNe, stellar winds or photoheating; no radiation pressure momentum flux; no feedback and radiation pressure boosted by 30. While global average GMC properties are similar in these models, the ratio of very dense to GMC gas mass, and hence the relative luminosity in tracers-like HCN, are sensitive to feedback. Gas heating has little effect on HCN because cooling times are so short at these densities, but adjusting the strength of radiation pressure leads to a nearly linear scaling in the predicted HCN luminosities. In our standard models, the predictions agree well with observations, both in the typical magnitude $L_{HCN}/L_{CO(1-0)}$ (a consequence of 'normal' feedback strength), and the trend with $L_{CO(1-0)}$, which stems from rising surface densities in more luminous systems.

a more accurate prediction would require a full non-local thermo-dynamic equilibrium (LTE) radiative transfer solution (outside the scope of this paper), and in any case, such a systematic offset does not change our conclusions. For example, we contrast the results with the choice of the surface density and metallicity-dependent α_{CO} derived in Narayanan et al. (2012), and obtain similar results.[1]

Because we cannot follow gas to arbitrarily high densities where SF actually occurs, the simulations enforce the observed relation between dense gas mass and SF efficiency (and indeed most of the SF occurs in gas with resolved densities $\gtrsim 10^4\,cm^{-3}$). This means

they automatically reproduce the observed L_{HCN}–SFR or L_{HCN}–L_{IR} relations: they define our SF prescription.[2]

However, Fig. 1 shows that the relative amount of high-density ($n \gtrsim 10^4\,cm^{-3}$) and intermediate-density/total molecular ($n \gtrsim 100\,cm^{-3}$) gas can vary dramatically. The relevant diagnostic is therefore the mass fraction in GMCs that is in dense cores, M_{dense}/M_{tot}, traced in $L_{HCN}/L_{CO(1-0)}$ or $L_{CO(3-2)}/L_{CO(1-0)}$. Fig. 2 plots this as a function of total cold gas mass $L_{CO(1-0)}$. For both tracers, we compare the observed relations:

$$\frac{L_{HCN}}{L_{CO(1-0)}} \propto 0.1 \left(\frac{L_{CO(1-0)}}{10^{10}\,K\,km\,s^{-1}\,pc^{-2}} \right)^{0.4}, \tag{1}$$

$$\frac{L_{CO(3-2)}}{L_{CO(1-0)}} \propto 0.1 \left(\frac{L_{CO(1-0)}}{10^{10}\,K\,km\,s^{-1}\,pc^{-2}} \right)^{0.5} \tag{2}$$

(Gao & Solomon 2004a; Narayanan et al. 2005).

---

[1] It is also not simply the case that these lines just trace the mass above a critical density. Evans (1999) advocate, for example, using instead the 'effective' density of tracers (the density needed to produce a line with radiation temperature of 1 K). We can re-consider our calculations using these densities, but we must be careful to also use the appropriate mass-to-light conversion calibrated for virial masses at these densities instead. From Wu et al. (2010), the effective density for HCN(1–0) is $n_{eff} \approx 5.1 \times 10^3\,cm^{-3}$, which for our standard SMC, MW, Sbc and HiZ models increases the total gas mass with $n > n_{eff}$ (relative to that with $n > n_{crit}$) by a factor of (1.7, 1.9, 4.5, 4.1), respectively. However the authors also re-calibrate the appropriate mass-to-light ratio (see their section 5.1), giving a best-fitting $L_{HCN}/M(n > n_{eff})$ conversion factor which is a factor ≈ 0.3 times our adopted $L_{HCN}/M(n > n_{crit})$. As a result, the predicted L_{HCN} is systematically different by only ≈ 50 per cent (slightly larger for the Sbc and HiZ models, smaller for the SMC and MW models). We see similar small changes in the simulations with varied feedback physics.

[2] If we arbitrarily raise/lower the efficiency of SF in the dense gas, we will systematically shift the amount of dense gas required for the SFR and corresponding feedback strength needed to self-regulate while preserving otherwise similar galaxy properties (this is shown explicitly in fig. 8 of Paper I). Hence this would also alter the density PDFs and L_{HCN}–L_{CO} relations in Figs 1 and 2, but at the expense of manifestly violating the observed L_{HCN}–SFR and L_{HCN}–L_{IR} relations. We investigate this in more detail below.

In the 'standard' (all feedback enabled) models, the predicted ratios of dense-to-cold gas and the scaling with gas mass/luminosity/SFR agree remarkably well with observations.

5 WHAT DETERMINES DENSE CORE FRACTIONS AND HCN LUMINOSITIES?

How does this scaling arise in our simulations? Dense clumps form and collapse until they produce sufficient stars such that the local feedback can offset gravity and disrupt the clump (generate a force $F_{\text{feedback}} \sim G M_{\text{cl}}^2/R^2 \sim G M_{\text{cl}} \Sigma_{\text{cl}}$). The total force needed to unbind the GMC is then $F_{\text{tot}} \sim G M_{\text{GMC}} \Sigma_{\text{GMC}}$. If all the feedback acting on the GMC is from young stars currently in dense clumps (and coupled therein), then the total force is simply the sum over the forces acting in each dense region i, $F_{\text{tot}} = \sum F_{\text{dense},i} = G \sum M_{\text{dense},i} \Sigma_{\text{dense},i} = G M_{\text{dense,tot}} \langle \Sigma_{\text{dense}} \rangle$. Equating the two gives $M_{\text{dense}}/M_{\text{GMC}} \sim \Sigma_{\text{GMC}}/\langle \Sigma_{\text{dense}} \rangle$.

More generally, the stars form in dense regions, but these can have a lifetime which is short compared to the massive stellar evolution time-scale (~ 5 Myr). For clumps that live for $N_t \sim 1$ free-fall times, the fraction of the GMC luminosity in dense clumps is $f_L \approx 0.1 n_4^{-1/2} N_t$, where $n_4 \equiv \langle n_{\text{cl}} \rangle / 10^4 \, \text{cm}^{-3}$.[3] As Fig. 1 shows, the dense gas is most affected by the local radiation pressure. The total force (momentum deposition rate) from radiation pressure in a (smooth) clump with average optical depth τ in the IR is $\dot{p} = (1 + \tau) L/c$; the total $\dot{p}$ in the GMC is then $(1 + [\tau_{\text{dense}} - \tau_0] f_L + \tau_0) L/c$ (where L is the total stellar luminosity, $\tau_0 = \kappa \Sigma_{\text{GMC}}$ is the mean τ of the GMC as a whole and $\tau_{\text{dense}} = \kappa \Sigma_{\text{dense}}$ is the mean τ of a dense clump).[4] We can estimate the required $L_{\text{cl}}/M_{\text{cl}}$ for each dense clump by again equating the force to gravity, and then $L = f_L^{-1} \sum L_{\text{cl}}$. Using this and equating the total force on the GMC to its self-gravity (and assuming $\tau_{\text{dense}} \gtrsim 1 \gg \tau_0$), we obtain

$$\frac{M_{\text{dense}}}{M_{\text{GMC}}} \approx \frac{f_L \tau_0}{1 + f_L \tau_{\text{dense}} + \tau_0} \tag{3}$$

$$\approx \frac{0.03 \, N_{t,3} \, n_4^{-1/2} \, \Sigma_{\text{GMC, 100}}}{1 + 0.3 \, N_{t,3} \, n_4^{-1/2} \, \Sigma_{\text{dense,1000}} + 0.1 \, \Sigma_{\text{GMC,100}}} \tag{4}$$

$$\rightarrow \frac{\Sigma_{\text{GMC}}}{\Sigma_{\text{dense}}} \quad (n_4^{-1/2} \, \Sigma_{\text{dense, 1000}} \gg 1), \tag{5}$$

where $N_{t,3} = N_t/3$, $\Sigma_{\text{GMC, 100}} \equiv \Sigma_{\text{GMC}}/100 \, \text{M}_\odot \, \text{pc}^{-2}$ [~ 1 for typical GMCs, i.e. in non-ultraluminous infrared galaxies (ULIRGs)],

---

[3] If the massive stars dominating the luminosity have lifetime $t_* \approx 5$ Myr, and clumps live for a time $t_{\text{cl}} \equiv N_t \, t_{\text{ff}} = N_t/\sqrt{(32/3\pi) \, G \, \rho_{\text{cl}}} \approx 0.5 \, N_t \, (n_{\text{cl}}/10^4 \, \text{cm}^{-3})^{-1/2}$ Myr, then (on average) if $t_{\text{cl}} < t_*$ the fraction of massive stars (light) in clumps is $f_L \sim t_{\text{cl}}/t_* \sim 0.1 \, n_4^{-1/2} \, N_t$.

[4] There is some debate in the literature regarding the exact form of the $\eta \sim (1 + \tau)$ prefix in the momentum flux $\eta L/c$ (see e.g. Krumholz & Thompson 2012, but also Kuiper et al. 2012). For our purposes in this derivation, it is simply an 'umbrella' term which should include all momentum flux terms (including radiation pressure in the UV and IR, stellar winds, cosmic rays, warm gas pressure from photoionization/photoelectric heating and early-time SNe). These other mechanisms will introduce slightly different functional dependencies in our simple derivation, if they are dominant, however, the total value of $\eta \sim$ a few is likely to be robust even if IR radiation pressure is negligible, leading to the same order of magnitude prediction. And we find that using a different form of the radiation pressure scaling which agrees quite well with that calculated in Krumholz & Thompson (2012) has only weak effects on our results (see Paper I, appendix B, Paper II, appendix A2 and Hopkins et al. 2012c, appendix A).

$\Sigma_{\text{dense, 1000}} \equiv \Sigma_{\text{dense}}/1000 \, \text{M}_\odot \, \text{pc}^{-2}$ (~ 1 for typical dense clumps) and $n_4 \equiv n_{\text{dense}}/10^4 \, \text{cm}^{-3}$.

In simulations, we find typical $N_t \approx 2$–4; if we assume a fixed SFR per free-fall time $\dot{M}_* = \epsilon_* M_{\text{dense}}/t_{\text{free-fall, dense}}$ and use the above derivation to obtain the critical L/M in a dense clump, we predict $N_t \approx 3 \, (0.05/\epsilon_*)$. These values agree well with observational estimates (Evans et al. 2009, and references therein). Thus up to some 'saturation' level when $n_4^{-1/2} \, \Sigma_{\text{dense, 1000}} \gg 1$, we expect $M_{\text{dense}}/M_{\text{GMC}} \propto \epsilon_*^{-1}$ (inversely proportional to the small-scale SF efficiency, if it is constant); we demonstrate this explicitly below.

Note that one might also expect a dependence on metallicity, since the opacities τ appear; however, accounting for it properly (assuming opacity scales linearly with metallicity), the dependence on metallicity cancels nearly completely.

The predicted ratio $M_{\text{dense}}/M_{\text{GMC}}$ increases with Σ_{GMC}. We saw in Paper II that Σ_{GMC} increases with average galaxy surface density (hence galaxy SFR and luminosity). This drives the trend of increasing $L_{\text{HCN}}/L_{\text{CO(1–0)}}$ at higher luminosities in Fig. 2. Observationally, from the baryonic Tully–Fisher relation ($R_{\text{g}} \propto M_{\text{g}}^{0.25-0.33}$) (e.g. Stark, McGaugh & Swaters 2009), we expect (for Jeans-scale clouds) average surface densities $\Sigma_{\text{GMC}} \propto M_{\text{g}}^{0.3-0.5}$ (which fits well the direct estimates in Paper II). This leads to the prediction that $L_{\text{HCN}}/L_{\text{CO(1–0)}} \propto L_{\text{CO(1–0)}}^{(0.3-0.5)}$ for 'normal' galaxies (with an upper limit when $M_{\text{dense}}/M_{\text{GMC}} \sim 1$). Similar considerations can be used to derive the observed IR-CO(1–0) scaling (Andrews & Thompson 2011).

Note that this argument assumes that Σ_{dense} *does not* increase with average galaxy surface density, or at least not as rapidly as Σ_{GMC} does. There is some observational evidence that, at the highest clump masses, Σ_{dense} does not increase with increasing clump mass (e.g. fig. 8 in Murray 2009).

This simple force argument also predicts, for example, that in local luminous infrared galaxies (LIRGs) and ULIRGs, where enhanced SF is driven by extremely dense nuclear concentrations of gas, and so Σ_{GMC} *must* be large (it must be at least the mean density), the dense gas fraction or $L_{\text{HCN}}/L_{\text{CO(1–0)}}$ will be systematically larger. This has been observed (Gao & Solomon 2004b; Narayanan et al. 2005; Evans et al. 2006; Bussmann et al. 2008). Moreover, we can estimate the magnitude of this enhancement: in typical ULIRG nuclei, where the effect will be most extreme, the surface densities reach $\Sigma \gtrsim 10^3 \, \text{M}_\odot \, \text{pc}^{-2}$, reaching the limit where $L_{\text{HCN}}/L_{\text{CO(1–0)}} \sim M_{\text{dense}}/M_{\text{GMC}} \sim \langle \Sigma \rangle/\Sigma_{\text{dense}} \sim 0.1$–1 (i.e. where the dense gas fractions saturate) a factor ~ 10 larger than that in normal galaxies. This agrees well with the enhancements in L_{HCN} observed for ULIRGs and dense relative to normal spiral galaxies in Gao & Solomon (2004b) and Juneau et al. (2009).

Finally, note that our choice to normalize the above scalings around $\sim 10^4 \, \text{cm}^{-3}$ is purely for convenience (since this is near the densities of interest for the tracers we discuss here). The simple scaling argument above admits a continuum of densities, with equation (3) applicable to a wide range of densities $n \gg n_{\text{GMC}}$. If the SFR per dynamical time in the dense gas (ϵ_*) is constant, then this simply predicts $M_{\text{dense}}(n > n_{\text{crit}})/M_{\text{GMC}} \propto n_{\text{crit}}^{-1/2}$ (up to the 'saturation level' noted above).

6 DENSE TRACERS VERSUS FEEDBACK

Based on the derivations above, we can guess how the HCN and CO luminosities will behave under various changes to the feedback model, shown in Fig. 2. Because it has little effect on the most dense gas, removing gas heating has a weak effect on the predicted

correlations, even in the MW and SMC models. Note that it can move systems *along* the correlations – it does so by globally regulating the mass in winds, and so the total mass forming GMCs and ultimately forming stars (e.g. absolute $L_{CO(1-0)}$). But within GMCs, heating has little effect, since the cooling time is so short. Removing the local direct radiation pressure momentum flux, however, has a much more dramatic effect, similar to removing all forms of feedback entirely. In both cases, there is little or nothing to resist runaway collapse inside the GMCs, and dense gas piles up until it saturates at fractions of order unity relative to the total GMC mass (Fig. 1). These produce order-of-magnitude or larger discrepancies with the observations (in the SMC and MW case, momentum flux from SNe resist complete collapse, but the amount of dense gas is still ~10 times too large for the observations). On the other hand, if we artificially boost the local radiation pressure strength by a large factor, the dense gas is all removed. If we repeat the derivations above, with the radiation pressure force multiplied uniformly by a factor η, the predicted M_{dense}/M_{GMC} in the non-saturated regime ($\Sigma_{GMC} \ll \Sigma_{dense}$) simply scales $\propto \eta^{-1}$. This is what we find – the predicted $L_{HCN}/L_{CO(1-0)}$ decreases approximately linearly in proportion to the 'boost' in feedback strength.

7 DENSE TRACERS VERSUS STAR FORMATION EFFICIENCIES

From the scaling in Section 5, we can also anticipate how the HCN and CO luminosities will behave as we change the small-scale SF law adopted in the simulations. This is shown explicitly in Fig. 3. Recall, as discussed above and shown in Papers I and II, changing the SF law in high-density gas has essentially no effect on the total SFR of the simulations. This is because SF is feedback regulated, so simply requires a balance between a certain number of young stars (hence total feedback input) and global collapse/dissipation.

In Fig. 3, we systematically vary the SF efficiency ϵ_* (SFR per dynamical time in dense gas with $n > 1000\,cm^{-3}$), by a factor of ~10^3. We also consider a different model in which the instantaneous local SF efficiency is set to either unity or zero depending on whether a given gas parcel is locally self-gravitating (at the resolution limit), which produces a time and volume-averaged efficiency of $\langle\epsilon_*\rangle \sim 2$ per cent but with large variability. Across all these models, we find a $\lesssim 20$ per cent change in the total time-averaged SFR. Here, we see similarly that there is also almost no effect on the intermediate-density gas, traced in $L_{CO(1-0)}$. However, there is a strong systematic trend in the amount of high-density gas, reflected in L_{HCN}. In order to globally self-regulate against runaway collapse, a certain total amount of feedback, hence total SFR, is needed; but to achieve the same SFR with systematically lower (higher) efficiency, a correspondingly larger (smaller) amount of dense gas must be present (see also Paper I, fig. 5). The scaling is roughly inverse with efficiency, $L_{HCN} \propto \epsilon_*^{-1}$.

Thus, the ratio of high-density to intermediate-density gas, in tracers such as $L_{HCN}/L_{CO(1-0)}$, is really a direct tracer of the amount of feedback per 'unit dense gas', i.e. the product of the feedback and SF efficiencies: $L_{HCN}/L_{CO(1-0)} \propto (\eta\,\epsilon_*)^{-1}$.

However, at fixed feedback strength but changing ϵ_*, recall that the total SFR (for otherwise identical galaxies) is the same, while the amount of dense gas changes. Hence a tracer of the ratio of dense gas to total SFR, e.g. L_{HCN}/L_{IR}, is able to independently constrain ϵ_* and break this degeneracy. Here, we find very good agreement between the predicted L_{HCN}/L_{IR} in our 'default' models with fixed $\epsilon_* = 0.015$, and/or in the model with variable (self-gravity dependent) efficiencies (since this produces a very similar average
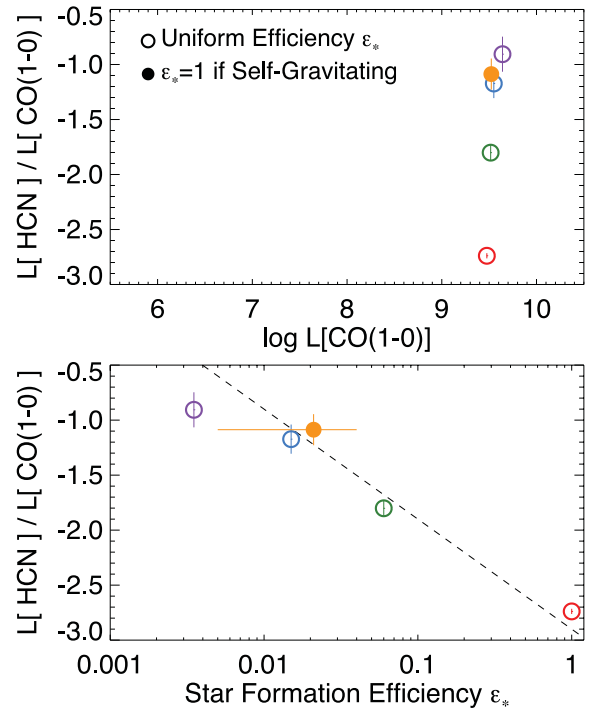
Figure 3. Dependence of dense-gas tracers on the small-scale SF efficiency ϵ_*. We show results for a series of otherwise identical simulations of the HiZ model, as in Fig. 2, but systematically vary the assumed simulation SF efficiency ϵ_* in the dense gas ($n > 1000\,cm^{-3}$), from which the SFR is $\dot\rho_* = \epsilon_* \rho_{mol}/t_{ff}$ (see Section 2). Top: very dense to GMC gas mass ratio as a function of GMC gas mass (as Fig. 2). Bottom: same HCN (1–0) to CO(1–0) ratio, for the same simulations, as a function of the SF efficiency ϵ_* assumed. The solid point does not assume a constant ϵ_*, but adopts the model in Hopkins, Narayanan & Murray (2013): the efficiency is $\epsilon_* = 1$ in regions which are locally self-gravitating, but $\epsilon_* = 0$ otherwise. We therefore plot the time and mass-averaged efficiency $\langle\epsilon_*\rangle$ predicted (with its scatter), around ~0.5–4 per cent. As shown in Paper I, the total SFR, total IR luminosity, and here, total CO luminosity (GMC gas mass) are nearly identical (insensitive to the small-scale SF law), because it is set by the SFR needed to balance collapse via feedback. However, to achieve the same SFR with lower (higher) efficiency, a larger (smaller) mass of dense gas is needed. The dense-to-GMC gas ratio scales approximately inversely with the mean $\langle\epsilon_*\rangle$ (dashed line shows a fit with slope $L[HCN]/L[CO(1-0)] \propto \langle\epsilon_*\rangle^{-1}$).

efficiency). Assuming fixed $\epsilon_* = 1$, on the other hand, leads us to predict a mean ratio L_{HCN}/L_{IR} a factor of ~50 lower than observed (in e.g. Gao & Solomon 2004a; Wu et al. 2010).

8 DISCUSSION

We have used a library of numerical hydrodynamic simulations of galaxies, with pc-scale resolution, molecular cooling and explicit spatial/time resolution of feedback mechanisms including radiation pressure in the UV and IR, supernovae, massive and AGB stellar winds and H II photoionization heating to study how the properties of dense gas – i.e. the gas where stars actually form – can be a sensitive tracer of the effects of feedback and a strong constraint on models of SF and stellar feedback. In Papers I and II, we show that these feedback mechanisms generically lead to the formation of a self-regulating, quasi-steady-state multiphase ISM, in which dense GMCs form via gravitational collapse. The GMCs then form clumps at densities $n > 10^4\,cm^{-3}$ in which most stars form. These stars, which have a total mass amounting to only a few per cent

of the GMC mass, then disrupt their parent GMCs. We showed in Paper II, however, that *most* properties of the ISM and GMCs are insensitive to the feedback mechanism or strength of feedback, so long as some mechanisms are present that are sufficient to resist runaway dissipation and collapse in these GMCs. Considering models with e.g. the dominant feedback mechanism being radiation pressure, SNe, H II photoheating or stellar winds; or models with different density thresholds, power-law dependencies or efficiencies of SF in dense subclumps; or models where we arbitrarily multiply/divide the strength of feedback by large factors; we find that provided something can make GMCs short-lived, their global properties (mass functions, densities, size–mass and linewidth–size relations, virial parameters and ISM velocity dispersions, scale-heights, phase structure and Toomre Q parameters) largely reflect global gravitational conditions rather than e.g. some local hydrostatic equilibrium that would be sensitive to the details of SF and/or feedback on small scales.

However, we show here that the properties of the very dense gas, $n \gtrsim 10^4$ cm^{-3}, *are* sensitive to the strength and nature of feedback, and the SF efficiency on small scales. If feedback is inefficient, then dense regions within GMCs will collapse and accrete until a large fraction of the GMC mass is in dense clumps. If, on the other hand, feedback is efficient, then only a small fraction of the dense clumps within a cloud collapse before sufficient massive stars are formed to unbind the parent cloud. If SF is inefficient, a 'bottleneck' appears and more gas must pile up at these densities to ultimately produce the same strength of feedback. The ratio of mass in dense gas – traced by dense molecular transitions such as L_{HCN} – to the total mass of cool gas – traced by lower density transitions such as $L_{CO(1-0)}$ – is therefore a sensitive measure of feedback and SF efficiencies. In models with weak or no feedback, we show that the predicted ratio $L_{HCN}/L_{CO(1-0)}$ is an order-of-magnitude or more larger than observed. In models with feedback efficiencies taken 'as is' from stellar evolution models, the predicted ratio agrees well with that observed. But if we arbitrarily make feedback more or less strong, multiplying the momentum flux by some factor η, then the predicted $L_{HCN}/L_{CO(1-0)}$ ratio scales approximately as η^{-1}; a model with 30 times stronger radiation pressure predicts ~30 times lower $L_{HCN}/L_{CO(1-0)}$.

Likewise, if the SF efficiencies either follow a physically motivated model where they reflect rapid collapse in only self-gravitating regions, or an imposed average ~1 per cent per free-fall time in the dense gas, then the predicted ratios agree well with the observations, but if we make the SF efficiency much lower (higher), the ratio of dense gas tracers to the total SFR (L_{HCN}/L_{IR}, for example) becomes much higher (lower) than observed. In some sense, then, the question of why SF efficiencies are low in a galaxy-wide sense is shifted to the question of why most very high-density gas is not forming stars rapidly (which these simulations cannot predict). Whether this is a consequence of 'slow' SF therein, or most such gas not being self-gravitating, or some additional physics not included here, remains an important subject for future work.

The predicted ratios are sensitive not just to the absolute strength of feedback, but also to the mechanisms of feedback. The thermal energy deposited by SNe explosions, for example, can have dramatic effects on galaxy scales (puffing up galaxy discs, driving turbulence and accelerating material into galactic superwinds), once it escapes from dense gas to efficiently heat low-density material. But it has almost no effect directly *within* the high-density gas, because the post-shock cooling time at these densities is ~10^4 times shorter than the dynamical time. We therefore predict that this mechanism has little effect on the observed $L_{HCN}-L_{CO(1-0)}$ relation, except to move galaxies *along* the relation by globally regulating the amount of (previously low-density) gas which can cool into new GMCs. Radiation pressure, on the other hand, can provide a very strong source of feedback at these densities, because these regions can be optically thick. Direct observations of massive star-forming regions have begun to suggest such a scenario (Lopez et al. 2011); correlating this with observations of the dense-to-low density gas mass ratio would provide a mechanism-specific diagnostic of feedback strength.

In addition to the normalization (median ratio L_{HCN}/L_{CO}), we show also that the systematic trends in $L_{HCN}-L_{CO}$ with e.g. SFR, L_{IR} or L_{CO} are tracers of feedback properties. We predict that the ratio of dense to total gas increases with increasing SFR and luminosity, in a manner in good agreement with observations. This arises because higher SFR systems tend to have higher cloud surface densities (equivalently, higher pressures) and therefore require more force (more SF, for the same feedback efficiencies) to unbind. We therefore predict a correlation between the dense gas ratio tracers and cloud surface densities of the form $\propto \Sigma_{GMC}$ (at low surface densities; it must saturate at higher densities), which should explain some of the observed scatter in nominal cloud lifetimes, dense gas formation efficiencies and measured SF efficiencies. This specifically predicts an enhanced ratio of $L_{HCN}/L_{CO(1-0)}$ in extreme systems such as ULIRGs and galaxy nuclei, and very high-redshift starburst discs – these systems have disc-average surface densities Σ in excess of the 'typical' MW Σ_{GMC}, so must have significantly higher Σ_{GMC}. This should also manifest in even higher density tracers such as HCN(3–2) (see e.g. Bussmann et al. 2008), for which our models here predict a more dramatic difference in the most extreme systems (but begins to push against our resolution limits). Such an enhancement has been tentatively observed; we provide a motivation for further observations to constrain how this scales with GMC and galaxy properties, as a means to directly constrain the efficiency of feedback as a function of these parameters.

ACKNOWLEDGEMENTS

REFERENCES

Andrews B. H., Thompson T. A., 2011, ApJ, 727, 97
Bournaud F., Elmegreen B. G., Teyssier R., Block D. L., Puerari I., 2010, MNRAS, 409, 1088
Bussmann R. S. et al., 2008, ApJ, 681, L73
Cullen L., Dehnen W., 2010, MNRAS, 408, 669
Dehnen W., Aly H., 2012, MNRAS, 425, 1068
Dobbs C. L., Burkert A., Pringle J. E., 2011, MNRAS, 413, 528
Durier F., Dalla Vecchia C., 2012, MNRAS, 419, 465
Evans N. J., II, 1999, ARA&A, 37, 311
Evans A. S., Solomon P. M., Tacconi L. J., Vavilkin T., Downes D., 2006, AJ, 132, 2398
Evans N. J. et al., 2009, ApJS, 181, 321
Gao Y., Solomon P. M., 2004a, ApJS, 152, 63
Gao Y., Solomon P. M., 2004b, ApJ, 606, 271

Harper-Clark E., Murray N., 2011, in Alves J., Elmegreen B. G., Girart J. M., Trimble V., eds, Proc. IAU Symp. 270, Computational Star Formation. Cambridge Univ. Press, Cambridge, p. 235

Hopkins P. F., 2012, MNRAS, 423, 2016

Hopkins P. F., 2013, MNRAS, 428, 2840

Hopkins P. F., Quataert E., Murray N., 2011, MNRAS, 417, 950 (Paper I)

Hopkins P. F., Quataert E., Murray N., 2012a, MNRAS, 421, 3488 (Paper II)

Hopkins P. F., Quataert E., Murray N., 2012b, MNRAS, 421, 3522

Hopkins P. F., Keres D., Murray N., Quataert E., Hernquist L., 2012c, MNRAS, 427, 968

Hopkins P. F., Narayanan D., Murray N., 2013, MNRAS, preprint (arXiv:1303.0285)

Juneau S., Narayanan D. T., Moustakas J., Shirley Y. L., Bussmann R. S., Kennicutt R. C., Jr, Vanden Bout P. A., 2009, ApJ, 707, 1217

Kennicutt R. C., Jr, 1998, ApJ, 498, 541

Kroupa P., 2002, Sci, 295, 82

Krumholz M. R., Gnedin N. Y., 2011, ApJ, 729, 36

Krumholz M. R., Tan J. C., 2007, ApJ, 654, 304

Krumholz M. R., Thompson T. A., 2007, ApJ, 669, 289

Krumholz M. R., Thompson T. A., 2012, ApJ, 760, 155

Krumholz M. R., Klein R. I., McKee C. F., 2011, ApJ, 740, 74

Kuiper R., Klahr H., Beuther H., Henning T., 2012, A&A, 537, A122

Lada C. J., Lombardi M., Alves J. F., 2010, ApJ, 724, 687

Leitherer C. et al., 1999, ApJS, 123, 3

Lopez L. A., Krumholz M. R., Bolatto A. D., Prochaska J. X., Ramirez-Ruiz E., 2011, ApJ, 731, 91

Mac Low M.-M., Klessen R. S., 2004, Rev. Modern Phys., 76, 125

Mannucci F., Della Valle M., Panagia N., 2006, MNRAS, 370, 773

Murray N., 2009, ApJ, 691, 946

Narayanan D., Groppi C. E., Kulesa C. A., Walker C. K., 2005, ApJ, 630, 269

Narayanan D., Cox T. J., Hernquist L., 2008a, ApJ, 681, L77

Narayanan D., Cox T. J., Shirley Y., Davé R., Hernquist L., Walker C. K., 2008b, ApJ, 684, 996

Narayanan D., Krumholz M. R., Ostriker E. C., Hernquist L., 2012, MNRAS, 421, 3127

Ostriker E. C., Stone J. M., Gammie C. F., 2001, ApJ, 546, 980

Saitoh T. R., Makino J., 2013, ApJ, 768, 44

Shirley Y. L., Evans N. J., II, Young K. E., Knez C., Jaffe D. T., 2003, ApJS, 149, 375

Springel V., 2005, MNRAS, 364, 1105

Stark D. V., McGaugh S. S., Swaters R. A., 2009, AJ, 138, 392

Tasker E. J., 2011, ApJ, 730, 11

Truelove J. K., Klein R. I., McKee C. F., Holliman J. H., II, Howell L. H., Greenough J. A., 1997, ApJ, 489, L179

Williams J. P., McKee C. F., 1997, ApJ, 476, 166

Wu J., Evans N. J., II, Gao Y., Solomon P. M., Shirley Y. L., Vanden Bout P. A., 2005, ApJ, 635, L173

Wu J., Evans N. J., II, Shirley Y. L., Knez C., 2010, ApJS, 188, 313

Yao L., Seaquist E. R., Kuno N., Dunne L., 2003, ApJ, 588, 771

Young J. S., Scoville N. Z., 1991, ARA&A, 29, 581

Zuckerman B., Evans N. J., II, 1974, ApJ, 192, L149

APPENDIX A: RESOLUTION AND NUMERICAL TESTS

Here we briefly discuss some numerical tests of the results in the paper.

In Papers I and II, we consider extensive resolution tests, and demonstrate that global quantities such as the galaxy SFR, and correspondingly total IR luminosity, as well as the closely related total mass at 'GMC densities' ($n \gtrsim 100\,\mathrm{cm}^{-3}$) and by extension CO(1–0) luminosities discussed in the text are well converged even if we downgrade our numerical resolution by an order of magnitude (see Paper I, figs 5, 9, 10 and 11; Paper II, appendix B and fig. B1; as well as Hopkins et al. 2012b, appendix A and fig. A3). In

these studies we have surveyed our range of galaxy models with independently varied spatial and mass resolution from an order of magnitude more poor than the standard parameters in this text, up to models with $>3 \times 10^8$ particles and sub-parsec resolution.

However, in this paper we also focus specifically on gas at much higher densities $\sim 10^4$–$10^5\,\mathrm{cm}^{-3}$, which is more challenging to resolve. In GADGET, the density around a given particle is specifically related to the SPH smoothing kernel size h_{sml} as $\rho_i = N_{\mathrm{NGB}}\, m_i / (4\pi/3\, h_{\mathrm{sml},\,i}^3)$, where m_i is the particle mass and N_{NGB} the number of SPH 'neighbours'. Thus resolving a density $n = n_4 \times 10^4\,\mathrm{cm}^{-3}$ requires minimum softening lengths $h_{\mathrm{sml}} \lesssim 8.5\, n_4^{-1/3}\, (m_i/10^4\,\mathrm{M}_\odot)^{1/3}$ pc (with 64 neighbours). This condition is satisfied, although in some cases, only by a relatively small margin, in all our runs at the critical densities used in the text. However, for such resolution to be meaningful, it also must be the case that the simulations can resolve the (turbulent) Jeans mass of structures with these densities (spurious collapse when this is not resolved is prevented by the standard Truelove et al. 1997 criterion; see Paper I for details). It is straightforward then to see that we are only just able to resolve these high densities in our fiducial runs.

Fig. A1 demonstrates this more explicitly by considering the gas density distribution in a series of HiZ runs with otherwise identical parameters but differing numerical resolution (a run both lower and higher resolution than our 'standard' resolution in the text). In each case, the mass and force resolution of the simulation effective sets a maximum resolvable density. At our fiducial resolution this maximum is a few $10^5\,\mathrm{cm}^{-3}$. If we increase our resolution in mass by almost an order of magnitude, this increases to $\sim 10^6\,\mathrm{cm}^{-3}$, and if we downgrade it by a similar amount, the density distribution cuts off at $\approx 10^5\,\mathrm{cm}^{-3}$. It does appear that at the critical densities $<10^5\,\mathrm{cm}^{-3}$, the results are converged (to within a margin substantially smaller than the scatter in time seen in the simulations). If we use the 'effective densities' of the high-density tracers (which are somewhat lower than the critical densities), the convergence is better. Clearly, however, going to even higher density tracers with criti-
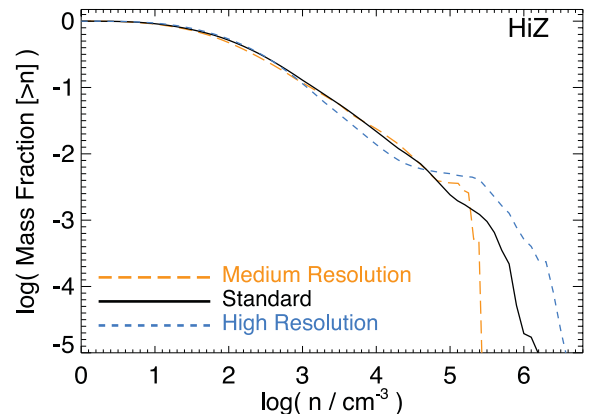
Figure A1. Cumulative density distributions from Fig. 1, in a resolution study of otherwise identical HiZ models. All examples are our default standard model (with all feedback mechanisms included). The 'standard resolution' case is run at the same resolution as the model in the main text (for the HiZ model, this is 5×10^6 gas particles with a force softening of 7 pc). We compare 'medium resolution' (1.2×10^6 gas particles, 11 pc force softening) and 'high resolution' (3×10^7 gas particles, 4 pc force softening). Medium/high resolution runs have also been run for the SMC and MW models, with the same gas particle numbers as those above, but force softenings $=0.2$ and 0.7 times smaller, respectively, with qualitatively similar results.

cal densities $\gtrsim 10^6$ cm^{-3} will require substantially higher resolution simulations.

We have also checked whether or not the details of the numerical method change our conclusions. We have re-run a subset of our simulations with the new 'pressure–entropy' formulation of smoothed particle hydrodynamics (SPH) developed in Hopkins (2013). This is an alternative formulation of the SPH equations which removes the spurious numerical 'surface tension' term and greatly improves the behaviour in treating certain fluid mixing instabilities (see also Saitoh & Makino 2013). This also eliminates most of the known discrepancies between the results of SPH and Eulerian grid-based simulations. As well, the new version of the code includes improvements in the smoothing kernel (Dehnen & Aly 2012), treatment of artificial viscosity (Cullen & Dehnen 2010) and time-stepping algorithm (Durier & Dalla Vecchia 2012). As shown in Hopkins (2013), however, these improvements make very little difference to the quantities of interest here (they mostly affect the mixing of diffuse, hot gas in galactic haloes); the SFR and dense gas distributions in the galaxies we simulate here are generally altered at the <20 per cent level.

This paper has been typeset from a TEX/LATEX file prepared by the author.